

Complete modes of star-shaped oscillating drops

Jiahao Dong,¹ Yuping Liu,² Qian Xu,^{1,*} Yinlong Wang,¹ and Sihui Wang^{1,†}

¹*School of Physics, Nanjing University, Nanjing 210093, China*

²*Kuang Yaming Honors School, Nanjing University, Nanjing 210093, China*

(Dated: December 31, 2018)

The star-shaped oscillation of water drops has been observed in various physical situations with different sources of vertical excitation. Previous studies apply a quasi-2D model to analyze the resonance frequency and only consider the azimuthal oscillation mode. In this paper, we find that the upper surface of water drops also develop different motion patterns due to parametric instability and it is the coupling of surface motion and azimuthal oscillation that leads to star-shaped oscillations. We will introduce the analysis of the surface mode, combining with the azimuthal mode to give a complete description of the motion of water drops. We propose a new dispersion relation based on the complete description, which provides a significant increase of accuracy in predicting the oscillating frequencies.

I. INTRODUCTION

Liquid drops driven by vertical excitation can develop star-shaped oscillations under certain conditions, including drops on a vertically vibrating hydrophobic plate [1], drops on a pulsating air cushion [2], acoustically levitating drops [3], metal drops placed on an oscillating magnetic field [4]. These oscillation systems are considered to undergo parametric resonance because the water drops are observed to oscillate in half of the frequency of the excitation source experimentally [3, 5, 6]. Even in the Leidenfrost effect [7–11] that the water drops are levitated by water vapor on a very hot plate, recent studies have found the periodically vibrating pressure of the vapor layer under the water drops can serve as parametric excitation [12, 13]. Despite these experimental evidences, the mechanism that induces the parametric instability is still unclear.

In the past, the oscillation modes of the flattened water drops are described by Rayleigh equation, proposed for inviscid cylindrical drops. The eigen frequencies for small deformations are given by [9, 14]:

$$\omega_n = \sqrt{\frac{n(n^2 - 1)\sigma}{\rho R^3}} \quad (1)$$

where n and ω_n represent azimuthal mode and corresponding eigen frequency respectively, and R is the balanced radius of the water drop, σ the surface tension constant, ρ the density of water. In the equation, the motion of the water drops is simplified as two-dimensional. Though the dispersion relation 1 gives right trend between the oscillation mode number n and the frequency, more detailed studies by Bouwhuis et al. [15] found that the measured resonance frequencies of star-shaped drops levitating on a steady ascending airflow are lower than

that given by 1, overestimating of the stiffness coefficient of the oscillating drop.

The two-dimensional model apparently oversimplifies the oscillation modes and loses accuracy when upper surface motion is appreciable. Shen et al. have already found that the upper surface develops petal-shaped motion patterns [3, 4, 16]. In our experiments, we also find that, with the increase of mode number n , the upper surface of the water drop becomes unstable and forms various patterns.

In this paper, we will present a complete theoretical model to derive the surface normal modes of the drop and combine the azimuthal oscillation modes to give a complete description of the motion of water drops. We verify that the vertical driving force induces an instability on the upper surface due to parametric resonance. The coupling of the surface motion and azimuthal oscillation leads to the appearance of star-shaped drops oscillating at half of the driving frequency. The surface oscillation will be described in much the way as the Faraday waves. Faraday waves are patterns of standing waves observed at the free surface, when a layer of liquid in a container is driven to vibrate vertically [17–20].

We will introduce a new mode number m , the surface mode number, and propose a new dispersion relation, in which the oscillation frequency of the water drop depends on both mode numbers n and m . The stiffness coefficient is reduced due to the additional surface mode, so that the eigen frequencies are lower than that 1 predicts. We also conduct experiments by exciting star-shaped oscillating drops on a hydrophobic vibrating substrate. Our dispersion relation can predict the oscillation frequencies with high accuracy.

II. THEORY

We consider the oscillation of water drops on a hydrophobic substrate, which vibrates periodically and serves as a vertical excitation. A water drop on a stable hydrophobic substrate is approximately a flattened cylinder with thickness about twice the capillary length

* qian.xu@smail.nju.edu.cn

† wangsihui@nju.edu.cn

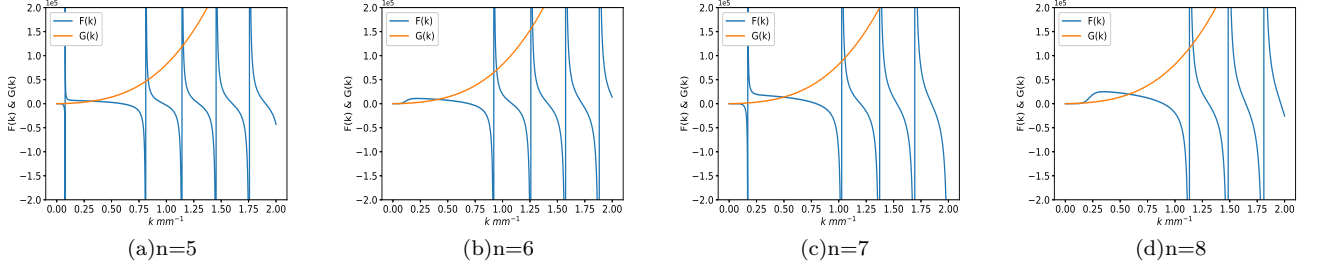


FIG. 1. $F(k)$ and $G(k)$ are plotted with orange and blue lines respectively, whose intersections determine the eigen values of k . From (a) to (d) azimuthal mode n increases from 5 to 8. $R = 10.8mm(2l_c)$, $\sigma = 72mN/m(25^\circ C)$.

($2l_c$), determined by a balance between the surface tension and the gravity [21].

We take cylindrical coordinates (r, θ, z) with respect to the frame of reference moving with the vibrating substrate, in which the undisturbed upper surface and periphery of the drop are $z = H$ and $r = R$ respectively. For an oscillating star-shaped drop, we use $h(r, \theta, t)$ and $a(z, \theta, t)$ to describe the small deviation of the upper surface and the periphery, hence the boundaries of the drop are described using $z = H + h$, $r = R + a$.

For irrotational liquid the velocity potential $\phi(r, \theta, z, t)$ [22] satisfies Eulerian equation

$$\frac{\partial \phi}{\partial t} + \frac{1}{2}(\nabla \phi)^2 + \frac{p}{\rho} + U = 0 \quad (2)$$

where $\nabla \phi$ is the fluid velocity, p is the internal pressure, U is the potential of external forces. For small movements of the water drop, we linearize the equation by omitting the term $(\nabla \phi)^2$.

The pressure at the free liquid surface [23] is

$$p = \sigma(\gamma_1 + \gamma_2) \quad (3)$$

where σ is the surface tension and γ_1, γ_2 are the principal radius of curvature (ROC) of the surface.

The ROCs of the upper surface can be obtained from membrane theory [24], by which we obtain $p = \sigma \nabla^2 h$. So the boundary condition of the upper surface is

$$\left(\frac{\partial \phi}{\partial t}\right)_{z=H+h} + \frac{\sigma}{\rho} \nabla^2 h + (g - F \cos(\Omega t)) h = 0 \quad (4)$$

Applying 3 to the periphery, we can get the boundary condition as

$$\left(\frac{\partial \phi}{\partial t}\right)_{r=R+a} - \frac{\sigma}{\rho R^2} \left(a + \frac{\partial^2 a}{\partial \theta^2}\right) = 0 \quad (5)$$

The bottom surface is in contact with the hydrophobic surface, thus the boundary condition is

$$\left(\frac{\partial \phi}{\partial z}\right)_{z=0} = 0 \quad (6)$$

Furthermore, at the liquid surfaces, $z = H + h$ and $r = R + a$, there are kinematic boundary conditions

$$\left(\frac{\partial \phi}{\partial z}\right)_{z=H+h} = \frac{\partial h}{\partial t} \quad (7)$$

$$\left(\frac{\partial \phi}{\partial r}\right)_{r=R+a} = \frac{\partial a}{\partial t} \quad (8)$$

Considering the incompressibility, the equation of continuity can be written as

$$\frac{\partial^2 \phi}{\partial r^2} + \frac{1}{r} \frac{\partial \phi}{\partial r} + \frac{1}{r^2} \frac{\partial^2 \phi}{\partial \theta^2} + \frac{\partial^2 \phi}{\partial z^2} = 0 \quad (9)$$

For small deformations, Eq. 9 and Eqs. 4, 5, 6 are variable-separable. The oscillation of a flattened cylinder drop can be decomposed on the Bessel basis. Hence the general solution of the velocity potential is

$$\phi = \sum_{k,n} \cosh(kz) J_n(kr) \sin(n\theta) A_{k,n}(t) \quad (10)$$

where J_n refers to Bessel function. Here $A_{k,n}(t)$ represents the time-related coefficient. Similarly, $h(r, \theta, t)$ and $a(z, \theta, t)$ can be expressed as

$$h = \sum_{k,n} J_n(kr) \sin(n\theta) B_{k,n}(t) \quad (11)$$

$$a = \sum_{k,n} \cosh(kz) \sin(n\theta) C_{k,n}(t) \quad (12)$$

Inserting Eqs. 10, 11 and 12 into Eqs. 7 and 8, the coefficients $A_{k,n}(t)$, $B_{k,n}(t)$ and $C_{k,n}(t)$ satisfy

$$\frac{dC_{k,n}(t)}{dt} = k J'_n(kR) A_{k,n}(t) \quad (13)$$

$$\frac{dB_{k,n}(t)}{dt} = k \sinh(kH) A_{k,n}(t) \quad (14)$$

Then substituting Eqs. 10, 11 and 12 to upper surface motion equation Eq. 4, we obtain

$$\frac{d^2 B_{k,n}}{dt^2} + k \tanh(kH) \left(g + \frac{\sigma k^2}{\rho} - F \cos \Omega t\right) B_{k,n}(t) = 0 \quad (15)$$

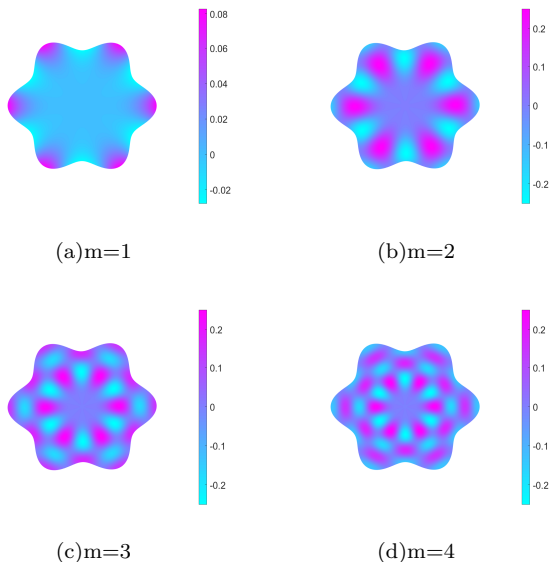


FIG. 2. Top views of the surface motion patterns (first four modes). The colormap of the surface corresponds to the height variation. The colorbars represent height (in mm). The corresponding values of k_m are $k_1 = 0.402mm^{-1}$, $k_2 = 0.915mm^{-1}$, $k_3 = 1.258mm^{-1}$ and $k_4 = 1.574mm^{-1}$. $n = 6$, $R = 10.8mm$ ($2l_c$) and $\sigma = 72mN/m$ ($25^\circ C$).

It's a parametric resonance equation, describing the response of the drop surface to the vertical excitation $F\cos\Omega t$. Here k can be regarded as a wave-vector of the upper surface. If we denote p and q as follow

$$p = \frac{k \tanh(kH)}{\Omega^2} \left(g + \frac{\sigma k^2}{\rho} \right) \quad (16)$$

$$q = \frac{kF \tanh(kH)}{\Omega^2} \quad (17)$$

Then Eq. 15 can be transformed to the standard form of Mathieu's equation

$$\frac{d^2 B_{k,n}}{dt^2} + (p + q \cos\Omega t) B_{k,n}(t) = 0 \quad (18)$$

The natural oscillating frequency ω of the system can be obtained by setting $\Omega = 0$. The principle subharmonic resonance occurs when [25]

$$\frac{\Omega^2}{4} - \frac{q}{2} < \omega^2 < \frac{\Omega^2}{4} + \frac{q}{2} \quad (19)$$

In practical cases, q is much smaller than p so that the resonance condition is simplified as $\omega \approx \Omega/2$. When the driving frequency is twice of the system natural frequency, the free surface becomes unstable and the surface oscillation mode increases in amplitude until it is finally restricted by damping or non-linear effects.

On the lateral surface, substituting Eqs. 10 and 12 into motion equation 5, we obtain

$$\frac{d^2 C_{k,n}}{dt^2} + \frac{(n^2 - 1)k\sigma J'_n(kR)}{\rho R^2 J_n(kR)} C_{k,n}(t) = 0 \quad (20)$$

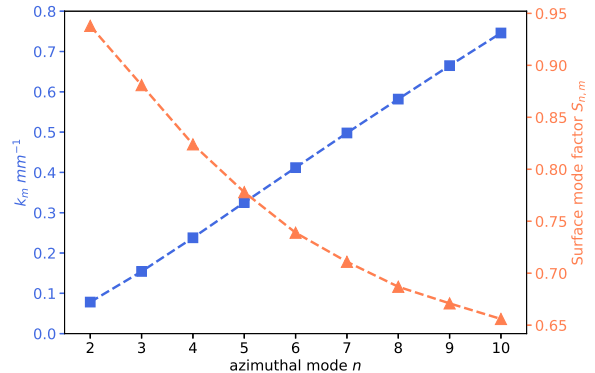


FIG. 3. Numerical calculation results of both k_m (orange triangles) and surface mode factor $S_{m,n}$ (blue squares). n increases from 2 to 10 and we take $m = 1$ for all values of n . $R = 10.8mm$ ($2l_c$), $\sigma = 72mN/m$ ($25^\circ C$).

Equation 20 defines a harmonic oscillating frequency of the drop periphery.

From 13 and 14 we know that, the induced surface motion due to parametric instability drives azimuthal motion in the same frequency ω and an azimuthal mode whose eigen frequency is in the vicinity of ω will be excited. Apparently, the two frequencies defined in Eqs. 15 and 20 should be equal, thus we obtain the eigen equation of k

$$\frac{(n^2 - 1)k\sigma J'_n(kR)}{\rho R^2 J_n(kR)} = k \tanh(kH) \left(g + \frac{\sigma k^2}{\rho} \right) \quad (21)$$

The eigen value k determines oscillation patterns of the surface. We use $F(k)$ and $G(k)$ to represent the left and right side of the equation 21, which are plotted together in figure 1. We find that $F(k)$ increases monotonically with k while $G(k)$ changes quasi-periodically. $F(k)$ and $G(k)$ have multiple intersections, and the m th nonzero intersection determines the m th eigen value k_m , which can be solved numerically. m also represents m th eigen mode of the upper surface. The pattern of the water drop is presented in figure 2, in which the height variation $h(r, \theta)$ of the upper surface is denoted with different colors for a $n = 6$ drop with m increasing from 1 to 4. Along the radial direction, the number of wave nodes is proportional to surface mode number m .

From Eqs. 20 and 21, n and m determine the resonance frequency of the water drop, so we have the dispersion relation

$$\omega_{m,n} = \sqrt{\frac{(n^2 - 1)k_m \sigma J'_n(k_m R)}{\rho R^2 J_n(k_m R)}} \quad (22)$$

When the surface motion is ignored, i.e. $k = 0$, we have the following equation

$$\lim_{k \rightarrow 0} \frac{k J'_n(kR)}{J_n(kR)} = \frac{n}{R} \quad (23)$$

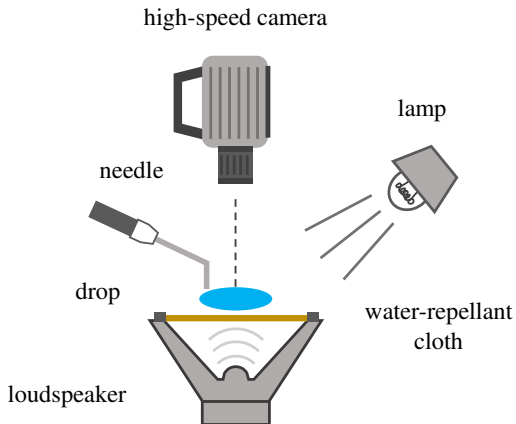


FIG. 4. Sketch of the experimental setup. The loudspeaker is driven by a signal generator. The needle places water drops on the hydrophobic cloth. The loudspeaker outputs low-frequency sound waves to excite the drops into oscillations. A high speed camera records the top view images.

Then equation 22 naturally reduces to Rayleigh equation 1. We define a factor $S_{n,m}$

$$S_{n,m} = \frac{\omega_{n,m}^2}{\omega_n^2} = \frac{R k_m J'_n(k_m R)}{n J_n(k_m R)} \quad (24)$$

It reflects the influence of the surface mode on the resonance frequency.

In figure 1, we can find that $m = 1$ and higher modes m have different oscillation frequencies. In practical cases, each oscillation frequency ω should correspond to one mode m . Usually, for the upper surface of the drop, higher-order modes are suppressed due to the dissipation of the system and an appreciable disturbance at the surface occurs only when a low-order mode is excited [19]. We numerically calculate k_m and $S_{m,n}$ for $m = 1$ and with n increasing from 2 to 10. As shown in figure 3, for drops with the same radius $R = 10.8mm$, the larger n , the larger the wave vector k_m , and the smaller the factor $S_{n,m}$ (all of them are smaller than 1), which corresponds to a more significant softening to resonance frequency.

For an oscillation system, the oscillating frequency is determined by the stiffness coefficient. The existence of surface modes would decrease the surface tension potential, consequently decreases the stiffness coefficient for the oscillation. Ignoring surface modes and reducing the motion of the water drop to two-dimensional overestimates the potential energy as well as the resonance frequency. We will compare the frequency to experimental results in the following section. And the correction also explains the discrepancy of oscillation frequency found in Ref. [15].

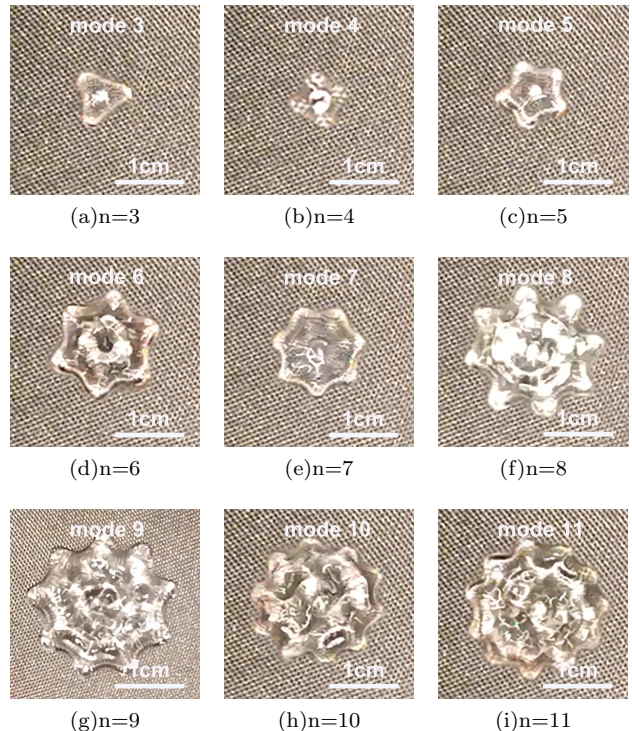


FIG. 5. Examples of instantaneous top views of star-shaped oscillating drops. From (a) to (i) the values of n increase from 3 to 11.

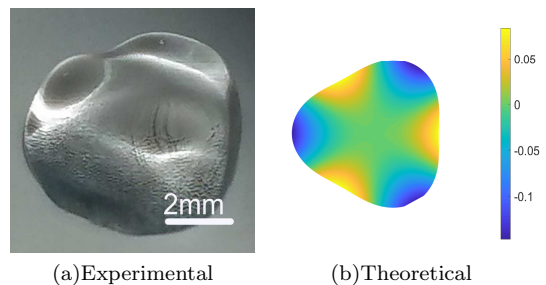


FIG. 6. (a) The surface pattern of a $n = 3$ drop captured from very close distance. We have enhanced the image contrast for visibility. (b) Corresponding theoretical surface mode ($m = 1$). The numerically solved wave-vector k_1 is $0.99mm^{-1}$. The height variation is denoted with different colors. The colorbar represents height (in mm).

III. EXPERIMENT AND RESULTS

Experimental setup is shown in Figure 4. A water-repellant cloth is attached horizontally to a loudspeaker cone (So-Voioe SVF149WR). For each drop the measured contact angle is more than 120° so that the hysteretic behavior can be avoided. The loudspeaker is connected to a signal generator (Right SG1020P), which applies a vertical excitation to the drop. We use an injector to control the volume and place the water drop on the cloth.

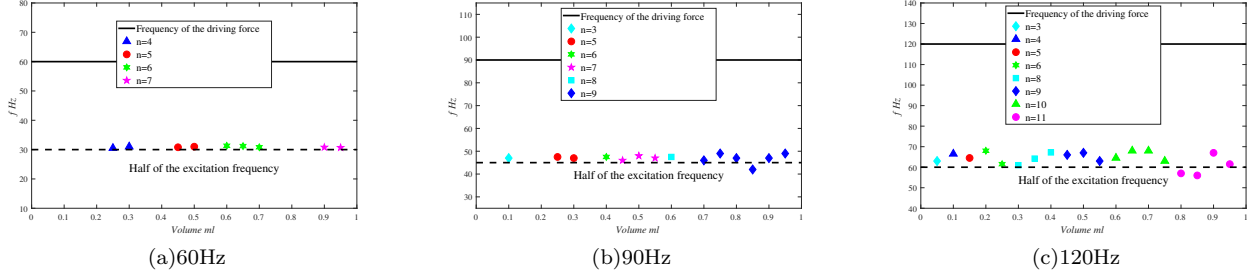


FIG. 7. Relation between the measured oscillation frequency f of star-shaped drops and half of the excitation frequency $f_0/2$. From (a) to (c) f_0 are $60Hz$, $90Hz$, and $120Hz$ respectively.

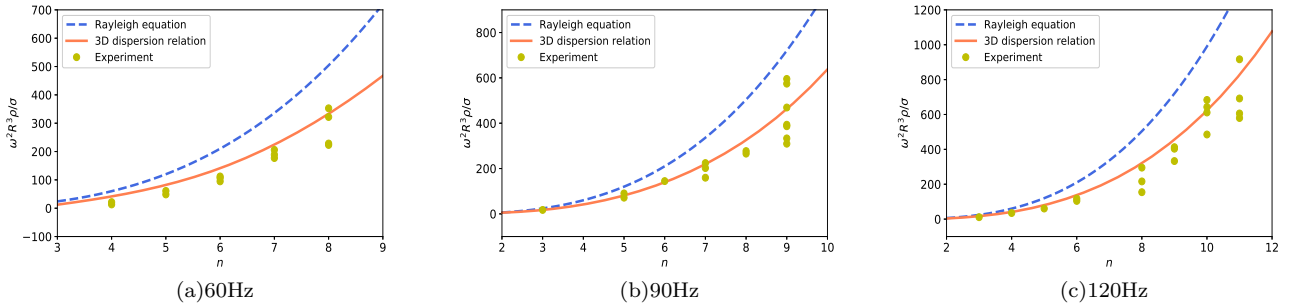


FIG. 8. Theoretically predicted values of $\omega^2 R^3 \sigma / \rho$ and experimental values. Blue dashed lines represent the values obtained from Rayleigh equation. Orange solid lines represent those obtained from the 3D dispersion relation (the data is calculated for each azimuthal mode n the line is connected using spline interpolation). Yellow dots are experimental values. From (a) to (c) f_0 are $60Hz$, $90Hz$, and $120Hz$ respectively.

The top view of the water drop is recorded using a high-speed video camera (Metalab 300C-U3) at the rate of 400 frames/s. When a drop performs stationary star-shaped oscillation, the camera records a sequence of images. The oscillating frequency f and mean radius R of the drop are analyzed frame by frame.

We set the input sinusoidal waves at the driving frequency $f_0 = \Omega/2\pi = 60Hz, 90Hz, 120Hz$ respectively. The volume of the water drop is increased by $0.05ml$ each time, measured by the injector. For $f_0 = 120Hz$, star-shaped oscillating drops from $n = 3$ to $n = 11$ are observed, as shown in figure 5. We can see the petal-like patterns at the upper surface, illustrating the existence of surface motion patterns. For $f_0 = 90Hz$, star-shaped drops $n = 3, 5, 6, 7, 8, 9$ are observed; for $f_0 = 60Hz$, star-shaped drops $n = 4, 5, 6, 7$ are observed. The surface mode computed with our model is compared to the experimental photograph for a $n = 3$ drop in figure 6. The radius of the drop is $2.7mm$ and the calculated wavevector k_1 is $0.99mm^{-1}$. The drop is captured from very close distance and we enhance the image contrast for visibility. The theoretical image resembles the experimental one. We show the relation between the measured oscillating frequency f and half of the excitation frequency $f_0/2$ in figure 7. The subharmonic parametric resonance condition 19 is satisfied.

In dispersion relation 1, the predicted value of ω^2 varies as $n(n^2 - 1)$, while in the new dispersion relation 22 we propose, it varies as $n(n^2 - 1)$ multiplied by an additional factor $S_{n,m}$. For each azimuthal mode n , we calculate the eigen value of k_m by solving equation 21 numerically and we take mode number $m = 1$. For $f_0 = 120Hz, 90Hz, 60Hz$, k_1 are calculated and equal to $1.4mm^{-1}, 1.0mm^{-1}, 0.8mm^{-1}$ respectively. We find k_1 appears to be independent of the azimuthal mode n , only determined by the excitation frequency f_0 . In figure 8 we plot the theoretical results according to 1 and 22, as well as the experimental results of $\omega^2 R^3 \sigma / \rho$. The yellow dots are experimental values. The blue dashed lines represent the values predicted by 1, obviously overestimating the oscillating frequency. And the orange solid lines represent those predicted by 22, which fits the experimental data much better. For some azimuthal number n the observed oscillation frequency consist of a set of data points. Actually these drops have the same azimuthal mode n but are slightly different in radius R and surface factor $S_{n,m}$. while we only substitute in 22 the average R observed in experiment.

IV. CONCLUSION

In this paper, we derive a complete theoretical model to include both surface modes and azimuthal modes of water drops under vertical excitation. The model we propose is applicable to drops under any form of vertical excitation. We prove that the star-shaped oscillation originates from parametric instability of the upper surface and explain the mechanism that leads to the star-shaped oscillation. We also propose a new dispersion relation based on the combination of surface modes and azimuthal modes, which gives a lower resonance frequency due to

the additional surface mode. The dispersion relation explains the discrepancy of oscillation frequencies found in previous studies and is in good agreement with our experimental data. These results enhance our understanding of the dynamics of water drops.

ACKNOWLEDGEMENTS

The authors are grateful to Mr. Y. Luo for beneficial discussions.

-
- [1] X. Noblin, A. Buguin, and F. Brochard-Wyart. Triplon modes of puddles. *Phys. Rev. Lett.*, 94:166102, Apr 2005.
 - [2] M. Papoular and C. Parayre. Gas-film levitated liquids: Shape fluctuations of viscous drops. *Phys. Rev. Lett.*, 78:2120–2123, Mar 1997.
 - [3] C. L. Shen, W. J. Xie, and B. Wei. Parametrically excited sectorial oscillation of liquid drops floating in ultrasound. *Phys. Rev. E*, 81:046305, Apr 2010.
 - [4] Y. FAUTRELLE, J. ETAY, and S. DAUGAN. Free-surface horizontal waves generated by low-frequency alternating magnetic fields. *Journal of Fluid Mechanics*, 527:285301, 2005.
 - [5] Nobuo Yoshiyasu, Kazuhisa Matsuda, and Ryuji Takaki. Self-induced vibration of a water drop placed on an oscillating plate. *J Phys Soc Jpn*, 65(7):2068–2071, jul 1996.
 - [6] P. Brunet and J.H. Snoeijer. Star-drops formed by periodic excitation and on an air cushion – a short review. *The European Physical Journal Special Topics*, 192(1):207–226, Feb 2011.
 - [7] David Qur. Leidenfrost dynamics. *Annual Review of Fluid Mechanics*, 45(1):197–215, 2013.
 - [8] Ken Adachi and Ryuji Takaki. Vibration of a flattened drop. i. observation. *Journal of the Physical Society of Japan*, 53(12):4184–4191, 1984.
 - [9] Ryuji Takaki and Ken Adachi. Vibration of a flattened drop. ii. normal mode analysis. *Journal of the Physical Society of Japan*, 54(7):2462–2469, 1985.
 - [10] Norman J. Holter and Wilford R. Glasscock. Vibrations of evaporating liquid drops. *The Journal of the Acoustical Society of America*, 24(6):682–686, 1952.
 - [11] D.E Strier, A.A Duarte, H Ferrari, and G.B Mindlin. Nitrogen stars: morphogenesis of a liquid drop. *Physica A: Statistical Mechanics and its Applications*, 283(1):261–266, 2000.
 - [12] Xiaolei Ma, Juan-José Liétor-Santos, and Justin C. Burton. Star-shaped oscillations of leidenfrost drops. *Phys. Rev. Fluids*, 2:031602, Mar 2017.
 - [13] Xiaolei Ma, Juan-Jos Litor-Santos, and Justin C. Burton. The many faces of a leidenfrost drop. *Physics of Fluids*, 27(9):091109, 2015.
 - [14] Lord Rayleigh. On the capillary phenomena of jets. *Proc.royal Soc.london*, 29:71–97, 1879.
 - [15] Wilco Bouwhuis, Koen G. Winkels, Ivo R. Peters, Philippe Brunet, Devaraj van der Meer, and Jacco H. Snoeijer. Oscillating and star-shaped drops levitated by an airflow. *Phys. Rev. E*, 88:023017, Aug 2013.
 - [16] Morihiro Okada and Minoru Okada. Observation of the shape of a water drop on an oscillating teflon plate. *Experiments in Fluids*, 41(5):789–802, Nov 2006.
 - [17] Michael Faraday. Xvii. on a peculiar class of acoustical figures; and on certain forms assumed by groups of particles upon vibrating elastic surfaces. *Philosophical Transactions of the Royal Society of London*, 121:299–340, 1831.
 - [18] Lord Rayleigh F.R.S. Xxxiii. on maintained vibrations. *The London, Edinburgh, and Dublin Philosophical Magazine and Journal of Science*, 15(94):229–235, 1883.
 - [19] T. B. Benjamin and F. Ursell. The stability of the plane free surface of a liquid in vertical periodic motion. *Proceedings of the Royal Society of London A: Mathematical, Physical and Engineering Sciences*, 225(1163):505–515, 1954.
 - [20] P. H. Wright and J. R. Saylor. Patterning of particulate films using faraday waves. *Review of Scientific Instruments*, 74(9):4063–4070, 2003.
 - [21] Anne-Laure Biance, Christophe Clanet, and David Qur. Leidenfrost drops. *Physics of Fluids*, 15(6):1632–1637, 2003.
 - [22] G. K. Batchelor. *An Introduction to Fluid Dynamics*. Cambridge Mathematical Library. Cambridge University Press, 2000.
 - [23] Sir Lamb, Horace. *Hydrodynamics*. Cambridge : Cambridge University Press, 6th ed edition, 1952. "Regarded as the sixth edition of a Treatise on the mathematical theory of the motion of fluids, published in 1879."–Pref.
 - [24] J.W.S.B. Rayleigh. *The Theory of Sound*, volume 1. Macmillan, 2nd ed edition, 1894.
 - [25] Insperger T. and Stépán G. Stability chart for the delayed mathieu equation. *Proceedings of the Royal Society of London. Series A: Mathematical, Physical and Engineering Sciences*, 458(2024):1989–1998, Aug 2002.